Highly Correlated Optomechanical Oscillations Manifested by an Anomalous Stabilization

Jinlian Zhang,[1] Miguel Orszag,[2] Min Xiao,[3] Xiaoshun Jiang,[3,*] Qing Lin,[1,†] and Bing He[2,‡]
[1]Fujian Key Laboratory of Light Propagation and Transformation and Institute of Systems Science, College of Information Science and Engineering, Huaqiao University, Xiamen 361021, China
[2]Center for Quantum Optics and Quantum Information, Universidad Mayor, Camino La Pirámide 5750, Huechuraba, Chile
[3]National Laboratory of Solid State Microstructures, College of Engineering and Applied Sciences, School of Physics, Nanjing University, Nanjing 210093, China

(Received 30 April 2024; revised 2 July 2024; accepted 6 August 2024; published 4 September 2024)

Driven by a sufficiently powerful pump laser, a cavity optomechanical system will stabilize in coupled oscillations of its cavity field and mechanical resonator. It was assumed that the oscillation will be continuously magnified upon enhancing the driving laser further. However, based on the nonlinear dynamics of the system, we find that the dynamical behaviors of the system are much more complex than this intuitive picture, especially when it is operated near the blue detuning point by the mechanical resonator's intrinsic frequency. There exists an anomalous stabilization: depending on its intrinsic damping rate and the pump power, the mechanical resonator will metastably stay on one orbit of oscillation after another until it completely stabilizes on the final orbit it can reach. These orbits are consistent with the locked ones with almost fixed oscillation amplitudes, which are realized after the pump power becomes still higher. The oscillatory cavity field is seen to adjust its sidebands following the mechanical frequency shift due to optical spring effect, so that it always drives the mechanical resonator to near those locked orbits once the pump power is over a threshold. In the regimes with such correlation between cavity field sidebands and mechanical oscillation, the system's dynamical attractors are confined on the locked orbits and chaotic motion is also excluded.

DOI: 10.1103/PhysRevLett.133.103602

Multiple oscillators coupled through nonlinear interaction potential exhibit nontrivial phenomena such as phase synchronization [1,2] and internal resonance of energy transfer [3,4]. When it comes to a pair of celestial bodies (two generalized oscillators), a complicated scenario can emerge: by its appropriate deformation and the adjustable gravitational interaction from the other, one of them will have its rotation and spin velocity locked to a fixed ratio (spin-orbit resonance) [5], explaining why the same side of the moon always faces Earth. Here, we illustrate that, through a unique mechanism realized by radiation pressure, a mechanical simple harmonic oscillator can be locked to a set of fixed orbits with its shifted frequency and a correspondingly adjusted light field spectrum.

So far, the effects of radiation pressure have been widely studied with cavity optomechanical systems (COMS) [6,7] exemplified in Fig. 1(a). Those effects are asymmetric with respect to the difference (detuning) of the driving laser frequency ω_l from the resonance frequency ω_c of the associated optical cavity. Scanning the pump frequency from the point red detuned by the mechanical frequency ω_m of a COMS, where the system can stabilize to a static equilibrium so that optomechanical cooling can be implemented [8–12], to where it is blue detuned by the same ω_m, one would encounter optomechanical oscillations [13–26] on the way: the mechanical resonator will stabilize in oscillation, while the cavity field is modulated to have more frequency components as the sidebands. On the other hand, a Hopf bifurcation determined by the pump power exists at a fixed drive frequency, as the boundary between static equilibrium and optomechanical oscillation. Viewed from the linearized dynamics, a two-mode squeezing effect is enhanced at the exact blue detuning by the mechanical frequency ω_m [7], which we call resonance point of blue detuning (RPB), and it could be beneficial for generating optomechanical entanglement [27–31]. A more powerful pump driving at a RPB was thus expected to always magnify the optomechanical oscillation further. However, based on the full nonlinear dynamics, the system driven at the RPB is found to stabilize in an anomalous way when the pump power is between one threshold higher than the Hopf bifurcation point and another transitional value toward a different regime of dynamics, resulting in a behavior contrary to the intuition that a stronger pump simply leads to more augmented optomechanical oscillation.

*Contact author: jxs@nju.edu.cn
†Contact author: qlin@hqu.edu.cn
‡Contact author: bing.he@umayor.cl

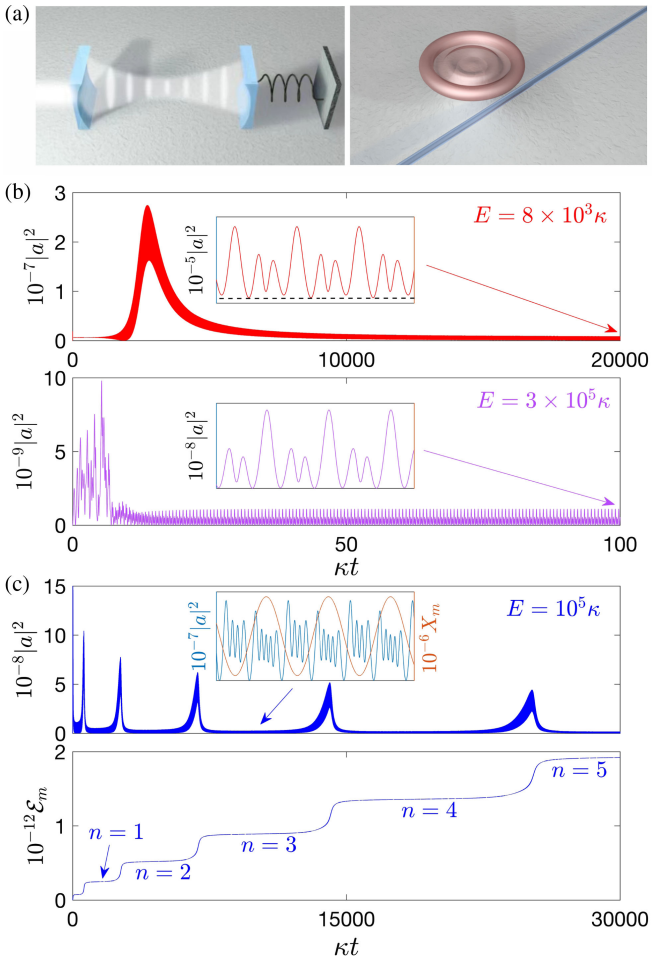

FIG. 1. (a) Two exemplary types of COMS: a movable mirror of Fabry-Perot cavity and the breathing mode of a microcavity driven through an optical fiber. (b) The normal stabilization processes of the intracavity photon number outside the AS regime and exactly at the RPB ($\Delta = -\omega_m$). The dashed line in the inset of the upper panel highlights a feature that the field oscillation does not split into two distinct parts in each whole period. (c) An anomalous stabilization at the RPB. Because of the pulsed $|a(t)|^2$ in succession, the metastable cavity field and mechanical oscillation repeatedly change together with time, manifesting the mechanical energy steps $n = 1$, 2, 3 and others. The lower (upper) limit for the AS phenomenon is around $E = 9.5 \times 10^3\kappa$ ($1.711\,399 \times 10^5\kappa$). Together with the indicated drive amplitudes E, the system parameters are all scaled by the damping rate κ: $g_m = 10^{-4}\kappa$, $\omega_m = 10\kappa$, and $\gamma_m = 0$.

For a realistic cavity, its displacement x_m under radiation pressure is much less than its original size, giving rise to an interaction potential $V(X_m) = -\hbar g_m X_m |a|^2$ for the coupled cavity field and mechanical resonator, where $|a|^2$ is the intracavity photon number and $X_m = \sqrt{(m\omega_m/\hbar)}x_m$ (m is the mechanical resonator's effective mass) is dimensionless. Then, the dynamical equations of the COMS are written in the reference frame rotating at the frequency ω_c as [32]

$$\dot{a} = -\kappa a + i g_m X_m a + E e^{i\Delta t}, \tag{1}$$

$$\ddot{X}_m = -\gamma_m \dot{X}_m - \omega_m^2 X_m + g_m \omega_m |a|^2, \tag{2}$$

where $\Delta = \omega_c - \omega_l$ is the laser detuning and its pump power P specifies the drive amplitude $E = \sqrt{2\kappa_e P/(\hbar\omega_l)}$. The mechanical damping rate γ_m can be much smaller than the field decay rate $\kappa = \kappa_e + \kappa_i$ from both pump-cavity coupling and intrinsic loss. To obtain an exact picture of dynamics, we will stick to the numerical calculations with Eqs. (1) and (2), together with some analytical arguments for interpreting the results.

An ideal situation is frictionless mechanical resonator ($\gamma_m = 0$); the whole coupled system stabilizes only under the field damping at a rate κ. Above the Hopf bifurcation point ($E \approx 1200\kappa$) at the RPB, such a system in Fig. 1 will enter oscillations. In most range of E, it is a normal stabilization (NS) showing a relatively short transient period, like the two processes in Fig. 1(b). However, after the amplitude E is switched to an in-between value as in Fig. 1(c), the system will undergo an anomalous stabilization (AS): the mechanical energy $\mathcal{E}_m(t) = \frac{1}{2}X_m^2(t) + \frac{1}{2}P_m^2(t)$ ($P_m = \dot{X}_m/\omega_m$) repeatedly jumps to a higher step, together with a field pattern change, after each action of a sequence of field pulses. The energy step heights are determined by the system's fabrication (mostly by the parameters g_m and ω_m).

The scenarios in Fig. 1(b) are outside the two boundaries of the AS regime illustrated in Fig. 2(a), which serves as a partial phase diagram at RPB. Although the pump power range between the boundaries of the AS regime is considerable to a specific COMS, the corresponding pump frequency range is narrow, e.g., within a window of 0.36κ at $(\omega_m/\kappa, g_m E/\kappa^2) = (10, 10)$; see Fig. 2(b). The mechanical energy steps and associated field patterns become deformed around the ratio $\omega_m/\kappa = 1$ [the purple point in the lower left-hand corner of Fig. 2(a)], and the phenomenon of AS gradually disappears with the further decreased $\omega_m/\kappa < 1$. If the ratio is tuned through fiber-cavity coupling to $\omega_m/\kappa = 1.1$ for the microresonator in Ref. [26], this remnant phenomenon of AS is observable with a pump power of 4.2 mW and within a frequency window of $2\pi \times 4.5$ MHz.

One can freely adjust the time lags between the pulses that push the mechanical oscillation to higher amplitudes. In Fig. 3(a) we show how to change the length of a mechanical energy step by the parameter $g_m E/\kappa^2$. For a specific COMS with fixed g_m, the pulses' emergence will be tremendously delayed if the pump power is close to both boundaries of the AS regime. It is due to the critical slowing-down near the bifurcation points. A realistic system ($\gamma_m \neq 0$) does not change the jump moments to the higher steps but will lower the gap,

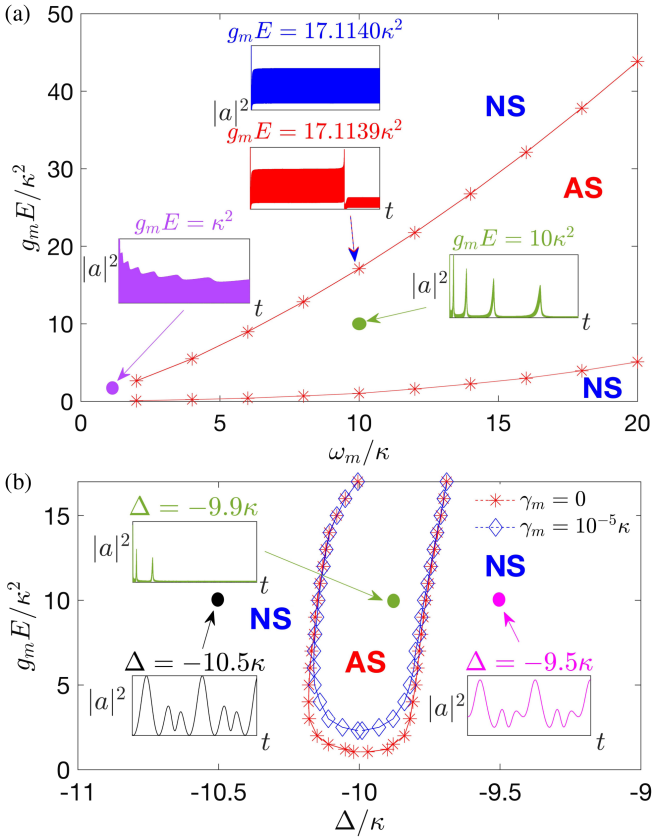

FIG. 2. (a) The distribution of the AS phenomenon in the space $(\omega_m/\kappa,\ g_mE/\kappa^2)$. The green and purple insets based on the parameters in Fig. 1 show the cavity field evolution over the duration of $\kappa t \in [0, 2\times 10^4]$ at the indicated points, and a transition across the upper boundary (the blue and red insets) is demonstrated within a duration $\kappa t \in [0, 5\times 10^4]$. Here the system driven at the RPB is the one with $\gamma_m = 0$. (b) The distribution of AS along the pump detuning. It is at the fixed $\omega_m/\kappa = 10$ in (a), where another exemplary system with $\gamma_m = 10^{-5}\kappa$ has the approximate lower (upper) boundary at $g_mE/\kappa^2 = 2.296$ (17.1139), while its Hopf bifurcation is around $g_mE/\kappa^2 = 0.2$. The duration of the green inset is still between $\kappa t = 0$ and 2×10^4, and those of two others are slightly over two mechanical oscillation periods.

$$\Delta\mathcal{E}_m(n) = \int_{\delta t_n} \{g_m|a(t)|^2 P_m(t) - \gamma_m P_m^2(t)\}dt, \quad (3)$$

between the $(n-1)$th and nth step by the second term of the above, with δt_n being the nth pulse's duration. For example, the mechanical damping up to $\gamma_m = 2.73\times 10^{-5}\kappa$ lowers the first step ($n = 1$) of the ideal system in Fig. 3(a) by about 1.2%. With a loss larger than this amount, the next pulse leading to $n = 2$ cannot be formed anymore and the resonator will stay on the former forever. A more general result is in Fig. 3(b): any realistic system operated in the AS regime stabilizes near one of a series of fixed average energy $\langle\mathcal{E}_m\rangle$ according to its mechanical damping rate γ_m and the optomechanical strength g_mE/κ^2, except for a sufficiently high γ_m that leads only to the dynamical processes below the lower boundary of the AS regime.

Before finally stabilizing on the step $n = 3$, a system with $\gamma_m = 10^{-5}\kappa$ and operated at $g_mE = 10\kappa^2$ temporarily stayed in two metastable states on $n = 1$ and $n = 2$ successively, having their corresponding cavity field patterns in Figs. 3(c1)–3(c3). Two factors explain why the system can be in these metastable and stable states during its time evolution. One is optical spring effect which shifts the actual frequency Ω_m of the mechanical oscillation $X_m(t) = \sqrt{2\langle\mathcal{E}_m\rangle}\cos(\Omega_m t) + d$ $(d/\sqrt{2\langle\mathcal{E}_m\rangle} \ll 1)$ by an amount $\delta = \Omega_m - \omega_m$. The other is the first sideband magnitude $A_1 = 2|\sum_{n=-\infty}^{+\infty} a_n^* a_{n+1}|$ of the field intensity or intracavity photon number,

$$|a(t)|^2 = \sum_{n=0}^{\infty} A_n \cos(n\Omega_m t + \phi_n), \quad (4)$$

where $a(t) = \sum_{n=-\infty}^{+\infty} a_n e^{i[\varphi(t)+n\Omega_m t]}$. Optical spring effect was regarded as a contribution to the effective spring constant $k_{\text{eff}} = m\omega_m^2 - (m\omega_m/\hbar)V''(X_0)$ by the radiation potential at the equilibrium position X_0 of the mechanical resonator, and there is an analytical form of δ based on the approximated linear response of COMS [7]. As a matter of fact, the mechanical resonator is generally under complicated radiation force during one oscillation period (see Fig. S-1 in Supplemental Material [32]), significantly deviating from the linear approximation. Instead, the shift δ can be exactly read from the Fourier transform of a numerically simulated $X_m(t)$ as in Figs. 3(c1)–3(c3). The sideband magnitude A_1, which can be obtained from the Fourier transform of $|a(t)|^2$, determines the energy,

$$\langle\mathcal{E}_m\rangle = \frac{(g_m\omega_m A_1)^2}{2\delta^2(2\omega_m+\delta)^2 + 2\gamma_m^2(\omega_m+\delta)^2}, \quad (5)$$

from Eq. (2). Generally one has $\delta \neq 0$, so the corresponding mechanical amplitude can be permanently or temporarily stable even for an ideal system with $\gamma_m = 0$. From Figs. 3(c1)–3(c3), the sideband magnitude A_1 dwindles after each jump of the mechanical amplitude. What compensates for the smaller driving force on a higher orbit is a further shrunk δ, so that the energy according to Eq. (5) will be the one on the higher orbit. The jointly reduced δ and A_1 in Fig. 3(c2) give $\langle\mathcal{E}_m\rangle = 5.21\times 10^{11}$, well close to 5.19×10^{11} on the level $n = 2$ in Fig. 4. In Fig. 3(c3) the system has reached a completely stable optomechanical oscillation after the mechanical frequency shift lowers to $\delta \sim \gamma_m$. More examples are two different $E = 2.5\times 10^4\kappa$ and $E = 1.7\times 10^5\kappa$, under both of which the COMS in Fig. 4 finally stabilizes on $n = 1$. Their corresponding $(\delta, A_1) = (2.48\times 10^{-5}\kappa, 3.373\times 10^5)$ and $(3.45\times 10^{-3}\kappa, 4.996\times 10^7)$ lead to the $\langle\mathcal{E}_m\rangle$ adequately near 2.476×10^{11} on the level $n = 1$. Through an automatic adjustment of δ with A_1, a system operating in the AS regime is

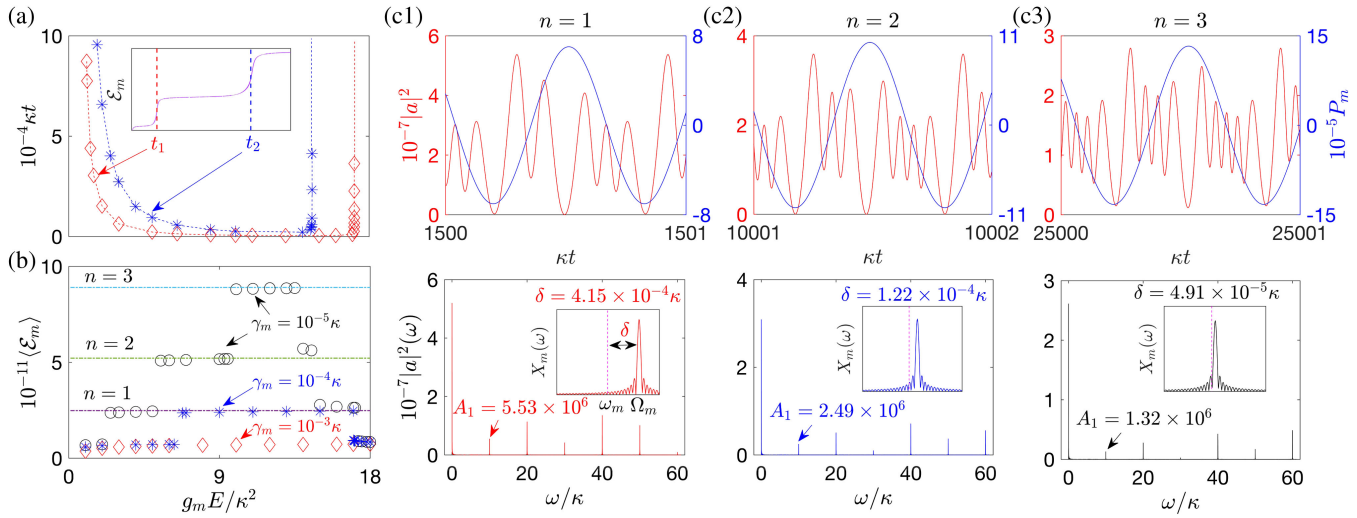

FIG. 3. (a) The adjustable moment t_1, corresponding to the driving pulse's peak, for an ideal system ($\gamma_m = 0$) to jump up to the step $n = 1$, together with the adjustable t_2 to the next $n = 2$, when this system of $g_m = 10^{-4}\kappa$ and $\omega_m = 10\kappa$ is driven at the RPB to have its mechanical energy evolution as in the inset. (b) The distribution of stabilized average energy $\langle\mathcal{E}_m\rangle$ (over one oscillation period) after adding various mechanical damping rates γ_m. The indicated levels are the average positions of the energy steps in (a), and are extremely close to those defined in Fig. 4. Panels (a) and (b) share the same horizontal axis. (c1)–(c3) The correlated field pattern and mechanical oscillation in both time domain and frequency domain, exemplified with the system operated at $g_m E/\kappa^2 = 10$ in (a) but with $\gamma_m = 10^{-5}\kappa$. On each step from $n = 1$ to $n = 3$, the metastable or stable $|a(t)|^2$ reaches its bottom value twice whenever the mechanical resonator arrives at its top speed in each oscillation period, forming a composite pattern of $2 + 3$, $3 + 4$, or $4 + 5$ peaks. Each lower panel displays the field intensity sideband magnitudes, together with the corresponding mechanical frequency shift in the inset.

always locked close to one of the reference energy levels like in Fig. 4.

The cavity field corresponding to the nth locked orbit has a special pattern of $(n + 1)$ plus $(n + 2)$ peaks during each mechanical oscillation period; see Figs. 3(c1)–3(c3). In contrast, the patterns in some NS regimes are noncompound, not splitting into two distinct parts in each oscillation period, like the stabilized one in the upper panel of Fig. 1(b). A field oscillation or its spectrum can be used to identify the associated mechanical orbit.

After the pump near the RPB becomes more powerful, the system will cross the upper boundary of the AS regime and be locked again to the more regularly distributed orbits (the levels $n = 1$, 2, 3 in Fig. 4 are according to the stabilized $\langle\mathcal{E}_m\rangle$ in this regime). Given the experimental setup in Ref. [26], the upper boundary at $\omega_m/\kappa = 10$ can be reached with a pump power around 55.5 mW. Now the system is in NS, but the possible field patterns still assume the composite ones as those in Figs. 3(c1)–3(c3). The lower panel of Fig. 1(b) displays one more composite pattern of $1 + 2$ peaks, corresponding to the lowest orbit $n = 0$. Those locked oscillations in the right-hand part of Fig. 4 are also due to the correlated A_1 and δ in Eq. (5). There exist random transitions between them under a slight change of the larger E in this regime, and they are similar to those caused by a two-tone drive with its tones differed by the mechanical frequency ω_m [33,34] (in that two-tone scenario a locked orbit similar to $n = 0$ is realized within the range of E for the AS regime).

One relevant issue is about the multiple dynamical attractors of a system driven at the fixed Δ and E. The mechanical amplitudes at the attractors were determined by the balanced average power flows into and out of a mechanical resonator [35–37], and such discrete mechanical amplitudes thus change with pump detuning and power continuously [32]. We approach the multistability by adding initial mechanical momentum to the dynamical processes described by Eqs. (1) and (2), so that the system can directly reach different basins of attraction. Apart from

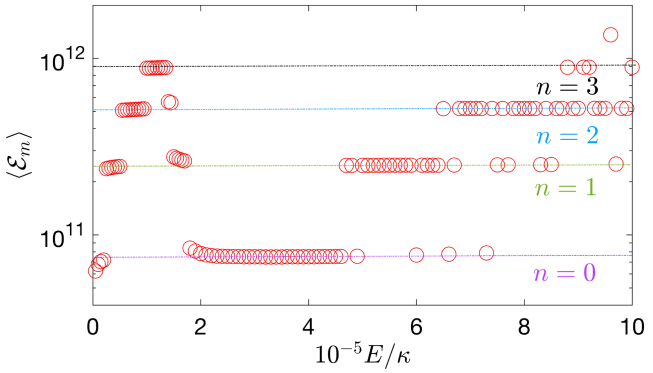

FIG. 4. The stabilized average mechanical energy distribution for a COMS driven at the RPB and from the static initial condition. From the left (AS regime) to the right (NS regime), the system is locked to the orbits from $n = 0$ to $n = 3$. The stray point in the upper right-hand corner is on $n = 4$. Here, $g_m = 10^{-4}\kappa$, $\omega_m = 10\kappa$, and $\gamma_m = 10^{-5}\kappa$.

below the lower boundary of the AS regime, where the attractors were observed by the signature of noncompound field patterns [38], we find that the attractors beside an RPB are totally locked to the fixed orbits like those in Fig. 4 [32]. Given enough pump power, locked orbits can exist in the vicinity of $\Delta = n\omega_m$ (n are integers). They exclude optomechanical chaos [39–43] to somewhere beyond the range of Fig. 4. Under lower drive powers, chaos emerges only at the detuning points without locked orbits, and one route toward this type of chaos is exemplified in Supplemental Material [32].

Although locked orbits can be encountered elsewhere over the detuning Δ of a pump laser, the phenomenon of AS is unique, only in a neighborhood of RPB. It is an effective channel to add up mechanical energy with lower pump powers. Not only the oscillations as phonon lasers [44–46] can be excited, coupling one COMS to other cavities will also preserve the phenomenon of AS, as long as the coupling intensities are below certain limit. It is possible for such coupled systems operating in the AS regime to outperform the $\mathcal{PT}$-symmetric phonon lasers [47–49] aided with optical gain.

Based on the full nonlinear dynamics well depicted by Eqs. (1) and (2), we have demonstrated that the dynamical behaviors of a COMS under single-tone drives are much richer than what were thought in the past, particularly near its RPB where only a Hopf bifurcation was known. In fact, responding to a continuously enhanced pump laser driving at the RPB, the system will first enter one more regime of AS and then another regime of NS. Like a celestial body deformation in tidal locking, a metastable or stable mechanical oscillation in these regimes is deformed by proper frequency shift, to correlate with the corresponding field sidebands, so that it can be locked to one of the reference energy levels as in Fig. 4, rather than its monotonous amplitude increase with the pump power higher than the Hopf threshold. The current understandings of optomechanical dynamics, especially the existence of AS processes, will find applications in the development of the relevant setups.

Acknowledgments—This research was supported by ANID Fondecyt Regular de Chile (Grant No. 1221250) and Natural Science Foundation of China (Grants No. 12374348, No. 12293054, No. 12341403).

[1] Y. Kuramoto, *Chemical Oscillations, Waves, and Turbulence* (Springer, Berlin, 1984).
[2] S. Boccaletti, A. N. Pisarchik, C. I. Del Genio, and A. Amann, *Synchronization: From Coupled Systems to Complex Networks* (Cambridge University Press, Cambridge, England, 2018).
[3] L. Manevitch and A. I. Manevich, *The Mechanics of Nonlinear Systems with Internal Resonances* (World Scientific, Singapore, 2005).
[4] A. K. Bajaj, P. Davies, and S. I. Chang, On internal resonances in mechanical systems, in *Nonlinear Dynamics and Stochastic Mechanics* (CRC Press, Boca Raton, FL, 2018), pp. 69–94.
[5] C. D. Murray and S. F. Dermott, *Solar System Dynamics* (Cambridge University Press, Cambridge, England, 1999).
[6] G. J. Milburn and M. J. Woolley, An introduction to quantum optomechanics, Acta Phys. Slovaca **61**, 483 (2011).
[7] M. Aspelmeyer, T. J. Kippenberg, and F. Marquardt, Cavity optomechanics, Rev. Mod. Phys. **86**, 1391 (2014).
[8] I. Wilson-Rae, N. Nooshi, W. Zwerger, and T. J. Kippenberg, Theory of ground state cooling of a mechanical oscillator using dynamical backaction, Phys. Rev. Lett. **99**, 093901 (2007).
[9] F. Marquardt, J. P. Chen, A. A. Clerk, and S. M. Girvin, Quantum theory of cavity-assisted sideband cooling of mechanical motion, Phys. Rev. Lett. **99**, 093902 (2007).
[10] A. Schliesser, O. Arcizet, R. Rivière, G. Anetsberger, and T. J. Kippenberg, Resolved-sideband cooling and position measurement of a micromechanical oscillator close to the Heisenberg uncertainty limit, Nat. Phys. **5**, 509 (2009).
[11] J. D. Teufel, T. Donner, D. Li, J. W. Harlow, M. S. Allman, K. Cicak, A. J. Sirois, J. D. Whittaker, K. W. Lehnert, and R. W. Simmonds, Sideband cooling micromechanical motion to the quantum ground state, Nature (London) **475**, 359 (2011).
[12] J. Chan, T. P. Mayer Alegre, A. H. Safavi-Naeini, J. T. Hill, A. Krause, S. Gröblacher, M. Aspelmeyer, and O. Painter, Laser cooling of a nanomechanical oscillator into its quantum ground state, Nature (London) **478**, 89 (2011).
[13] H. Rokhsari, T. J. Kippenberg, T. Carmon, and K. J. Vahala, Radiation pressure-driven micro-mechanical oscillator, Opt. Express **13**, 5293 (2005).
[14] T. Carmon, H. Rokhsari, L. Yang, T. J. Kippenberg, and K. J. Vahala, Temporal behavior of radiation-pressure-induced vibrations of an optical microcavity phonon mode, Phys. Rev. Lett. **94**, 223902 (2005).
[15] T. J. Kippenberg, H. Rokhsari, T. Carmon, A. Scherer, and K. J. Vahala, Analysis of radiation-pressure induced mechanical oscillation of an optical microcavity, Phys. Rev. Lett. **95**, 033901 (2005).
[16] C. Metzger, M. Ludwig, C. Neuenhahn, A. Ortlieb, I. Favero, K. Karrai, and F. Marquardt, Self-induced oscillations in an optomechanical system driven by bolometric backaction, Phys. Rev. Lett. **101**, 133903 (2008).
[17] S. Zaitsev, A. K. Pandey, O. Shtempluck, and E. Buks, Forced and self-excited oscillations of an optomechanical cavity, Phys. Rev. E **84**, 046605 (2011).
[18] J. B. Khurgin, M. W. Pruessner, T. H. Stievater, and W. S. Rabinovich, Optically pumped coherent mechanical oscillators: The laser rate equation theory and experimental verification, New J. Phys. **14**, 105022 (2012).
[19] M. Poot, K. Y. Fong, M. Bagheri, W. H. P. Pernice, and H. X. Tang, Backaction limits on self-sustained optomechanical oscillations, Phys. Rev. A **86**, 053826 (2012).
[20] O. Suchoi, L. Ella, O. Shtempluk, and E. Buks, Intermittency in an optomechanical cavity near a subcritical Hopf bifurcation, Phys. Rev. A **90**, 033818 (2014).

[21] C. Wurl, A. Alvermann, and H. Fehske, Symmetry-breaking oscillations in membrane optomechanics, Phys. Rev. A **94**, 063860 (2016).
[22] M.-A. Miri, G. D'Aguanno, and A. Alù, Optomechanical frequency combs, New J. Phys. **20**, 043013 (2018).
[23] Q. Lin, B. He, and M. Xiao, Catastrophic transition between dynamical patterns in a phonon laser, Phys. Rev. Res. **3**, L032018 (2021).
[24] P. Piergentili, W. Li, R. Natali, N. Malossi, D. Vitali, and G. Di Giuseppe, Two-membrane cavity optomechanics: Non-linear dynamics, New J. Phys. **23**, 073013 (2021).
[25] S. Christou, V. Kovanis, A. E. Giannakopoulos, and Y. Kominis, Parametric control of self-sustained and self-modulated optomechanical oscillations, Phys. Rev. A **103**, 053513 (2021).
[26] Y. Hu, S. Ding, Y. Qin, J. Gu, W. Wan, M. Xiao, and X. Jiang, Generation of optical frequency comb via giant optomechanical oscillation, Phys. Rev. Lett. **127**, 134301 (2021).
[27] T. A. Palomaki, J. D. Teufel, R. W. Simmonds, and K. W. Lehnert, Entangling mechanical motion with microwave fields, Science **342**, 710 (2013).
[28] Q. Lin, B. He, R. Ghobadi, and C. Simon, Fully quantum approach to optomechanical entanglement, Phys. Rev. A **90**, 022309 (2014).
[29] Q. Lin and B. He, Optomechanical entanglement under pulse drive, Opt. Express **23**, 24497 (2015).
[30] K. Y. Dixon, L. Cohen, N. Bhusal, C. Wipf, J. P. Dowling, and T. Corbitt, Optomechanical entanglement at room temperature: A simulation study with realistic conditions, Phys. Rev. A **102**, 063518 (2020).
[31] Q. Lin, B. He, and M. Xiao, Entangling two macroscopic mechanical resonators at high temperature, Phys. Rev. Appl. **13**, 034030 (2020).
[32] See Supplemental Material at http://link.aps.org/supplemental/10.1103/PhysRevLett.133.103602 for more details.
[33] B. He, Q. Lin, M. Orszag, and M. Xiao, Mechanical oscillations frozen on discrete levels by two optical driving fields, Phys. Rev. A **102**, 011503(R) (2020).
[34] Y. Wu, G. Li, B. He, and Q. Lin, Amplitude and phase locking of mechanical oscillation driven by radiation pressure, Phys. Rev. A **105**, 013521 (2022).
[35] F. Marquardt, J. G. E. Harris, and S. M. Girvin, Dynamical multistability induced by radiation pressure in high-finesse micromechanical optical cavities, Phys. Rev. Lett. **96**, 103901 (2006).
[36] M. Ludwig, B. Kubala, and F. Marquardt, The optomechanical instability in the quantum regime, New J. Phys. **10**, 095013 (2008).
[37] P. Djorwe, J. Y. Effa, and S. G. Nana Engo, Multistability, staircases, and optical high-order sideband combs in optomechanics, J. Opt. Soc. Am. B **37**, A36 (2020).
[38] F. M. Buters, H. J. Eerkens, K. Heeck, M. J. Weaver, B. Pepper, S. de Man, and D. Bouwmeester, Experimental exploration of the optomechanical attractor diagram and its dynamics, Phys. Rev. A **92**, 013811 (2015).
[39] T. Carmon, M. C. Cross, and K. J. Vahala, Chaotic quivering of micron-scaled on-chip resonators excited by centrifugal optical pressure, Phys. Rev. Lett. **98**, 167203 (2007).
[40] L. Bakemeier, A. Alvermann, and H. Fehske, Route to chaos in optomechanics, Phys. Rev. Lett. **114**, 013601 (2015).
[41] D. Navarro-Urrios, N. E. Capuj, M. F. Colombano, P. D. Garcia, M. Sledzinska, F. Alzina, A. Griol, A. Martinez, and C. M. Sotomayor-Torres, Nonlinear dynamics and chaos in an optomechanical beam, Nat. Commun. **8**, 14965 (2017).
[42] T. F. Roque, F. Marquardt, and O. M. Yevtushenko, Nonlinear dynamics of weakly dissipative optomechanical systems, New J. Phys. **22**, 013049 (2020).
[43] G.-L. Zhu, C.-S. Hu, Y. Wu, and X.-Y. Lü, Cavity optomechanical chaos, Fundam. Res. **3**, 63 (2023).
[44] I. S. Grudinin, H. Lee, O. Painter, and K. J. Vahala, Phonon laser action in a tunable two-level system, Phys. Rev. Lett. **104**, 083901 (2010).
[45] G. Z. Wang, M. M. Zhao, Y. C. Qin, Z. Q. Yin, X. S. Jiang, and M. Xiao, Demonstration of an ultra-low-threshold phonon laser with coupled microtoroid resonators in vacuum, Photonics Res. **5**, 73 (2017).
[46] J. Zhang, B. Peng, S. K. Özdemir, K. Pichler, D. O. Krimer, G. P. Zhao, F. Nori, Y. X. Liu, S. Rotter, and L. Yang, A phonon laser operating at an exceptional point, Nat. Photonics **12**, 479 (2018).
[47] H. Jing, S. K. Özdemir, X. Y. Lü, J. Zhang, L. Yang, and F. Nori, PT-symmetric phonon laser, Phys. Rev. Lett. **113**, 053604 (2014).
[48] B. He, L. Yang, and M. Xiao, Dynamical phonon laser in coupled active-passive microresonators, Phys. Rev. A **94**, 031802(R) (2016).
[49] Y. F. Xie, Z. Cao, B. He, and Q. Lin, PT-symmetric phonon laser under gain saturation effect, Opt. Express **28**, 22580 (2020).